

## Article

# Biocatalytic Cascade of Sebacic Acid Production with In Situ Co-Factor Regeneration Enabled by Engineering of an Alcohol Dehydrogenase

Jie Lu <sup>1,2</sup>, Dong Lu <sup>1,2</sup>, Qiuyang Wu <sup>1,2</sup>, Shuming Jin <sup>1,2</sup>, Junfeng Liu <sup>1</sup>, Meng Qin <sup>1</sup> , Li Deng <sup>1,2</sup>, Fang Wang <sup>1,2</sup> and Kaili Nie <sup>1,2,\*</sup> 

<sup>1</sup> College of Life Science and Technology, Beijing University of Chemical Technology, Beijing 100029, China

<sup>2</sup> Beijing Key Lab of Bioprocess, National Energy R&D Center for Biorefinery, Beijing University of Chemical Technology, Beijing 100029, China

\* Correspondence: niekl@mail.buct.edu.cn

**Abstract:** Sebacic acid (1,10-decanedioic acid) is an important chemical intermediate. Traditional chemical oxidation methods for sebacic acid production do not conform with “green” manufacturing. With the rapid development of enzymatic technologies, a biocatalytic cascade method based on the Baeyer–Villiger monooxygenase was developed. The most attractive point of the method is the oleic acid that can be utilized as raw material, which is abundant in nature. However, this bio-catalysis process needs co-factor electron carriers, and the high cost of the co-factor limits its progress. In this piece of work, a co-factor in situ regeneration system between ADH from *Micrococcus luteus* WIUJH20 (*MIADH*) and BVMO is proposed. Since the co-factors of both enzymes are different, switching the co-factor preference of native *MIADH* from NAD<sup>+</sup> to NADP<sup>+</sup> is necessary. Switching research was carried out based on in silico simulation, and the sites of Tyr36, Asp 37, Ala38, and Val39 were selected for mutation investigation. The experimental results demonstrated that mutants of *MIADH\_D37G* and *MIADH\_D37G/A38T/V39K* would utilize NADP<sup>+</sup> efficiently, and the mutant of *MIADH\_D37G/A38T/V39K* demonstrated the highest sebacic acid yield with the combination of BVMO. The results indicated that the in situ co-factor generation system is successfully developed, which would improve the efficiency of the biocatalytic cascade for sebacic acid production and is helpful for simplifying product isolation, thus, reducing the cost of the enzymatic transformations process.

**Keywords:** co-factor regeneration; alcohol dehydrogenase; sebacic acid; enzymatic cascade reaction; in silico simulation



**Citation:** Lu, J.; Lu, D.; Wu, Q.; Jin, S.; Liu, J.; Qin, M.; Deng, L.; Wang, F.; Nie, K. Biocatalytic Cascade of Sebacic Acid Production with In Situ Co-Factor Regeneration Enabled by Engineering of an Alcohol Dehydrogenase. *Catalysts* **2022**, *12*, 1318. <https://doi.org/10.3390/catal12111318>

Academic Editor: Albert Poater

Received: 26 September 2022

Accepted: 24 October 2022

Published: 27 October 2022

**Publisher's Note:** MDPI stays neutral with regard to jurisdictional claims in published maps and institutional affiliations.

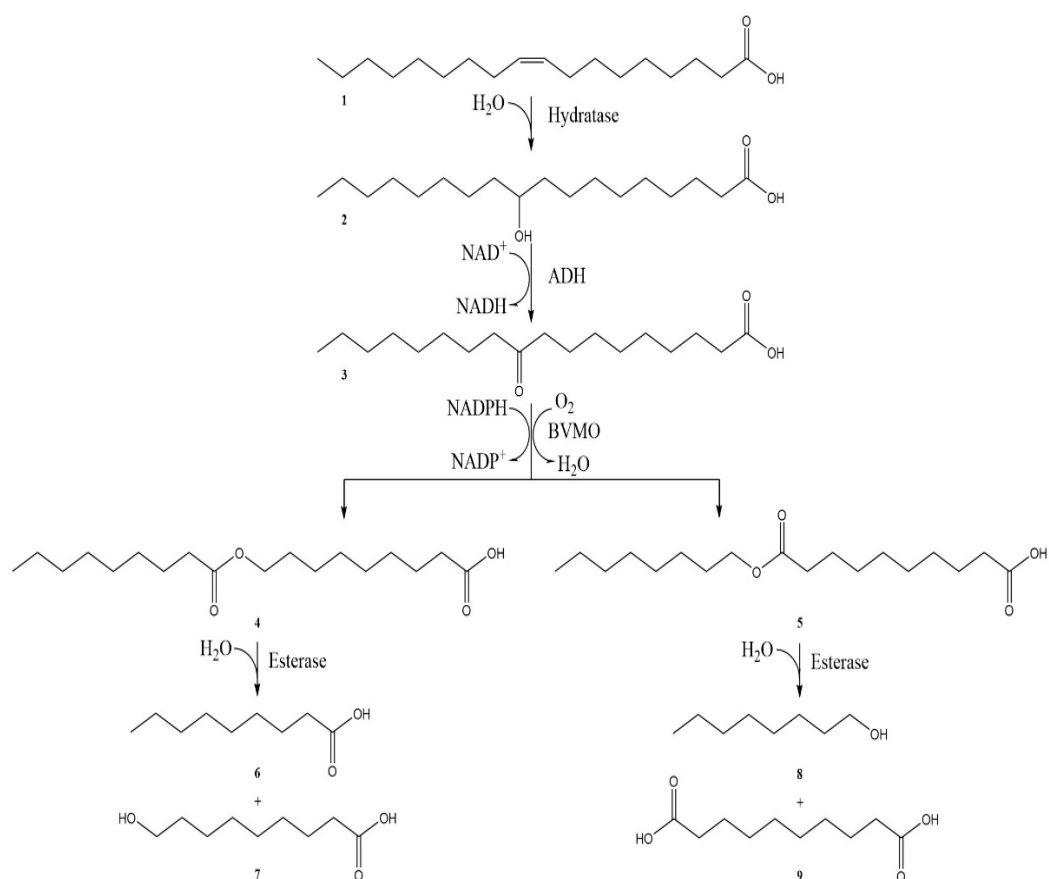


**Copyright:** © 2022 by the authors. Licensee MDPI, Basel, Switzerland. This article is an open access article distributed under the terms and conditions of the Creative Commons Attribution (CC BY) license (<https://creativecommons.org/licenses/by/4.0/>).

## 1. Introduction

Long-chain  $\alpha$ ,  $\omega$ -dicarboxylic acids ( $\alpha$ ,  $\omega$ -DCAs) are frequently and widely applied to produce various chemicals and intermediates, such as nylon, preservatives, lubricants, plasticizers, fragrances, and cosmetics [1]. Traditionally,  $\alpha$ ,  $\omega$ -DCAs are produced from petrochemical raw materials or special fatty acids (ricinoleic acid) through oxidative cracking with harsh reaction conditions, involving high temperature, high pressure, strong acid catalysts (e.g., H<sub>2</sub>SO<sub>4</sub>, HNO<sub>3</sub>), and toxic oxidants (e.g., ozone, peroxide) [2,3]. Due to the uncontrolled reaction, the process always had low yields, high energy consumption, and uncontrollable by-products, which were seriously harmful for the environment and did not meet the modern topic of “green and sustainable development” [4]. By contrast, enzymatic synthesis could be an alternative with advantages of having mild conditions; being environmentally friendly; and having high regio-, stereo-, and enantioselectivity [5]. Therefore, exploring a novel biocatalytic synthesis of  $\alpha$ ,  $\omega$ -DCAs is a subject of profound significance.

In recent years, there are more and more reports on cascade biocatalytic reactions. The advantages of cascade reactions are as follows: (1) the multi-step reaction can be carried out in a reactor and does not require the separation of intermediates; (2) less solvents and chemicals are needed; (3) intermediates are quickly consumed in continuous steps, which can reduce waste emissions. Therefore, cascade biocatalytic reactions can shorten the reaction time and cost [6,7]. Song et al. reported an enzymatic cascade process (Scheme 1, [8]) for sebacic acid (1,10-decanedioic acid, Compound 9) production with oleic acid (Compound 1) as raw material, which is a natural unsaturated fatty acid present in most kinds of vegetable oils. In this cascade reaction, hydratase hydrates the unsaturated carbon–carbon double bond of oleic acid firstly, and then the hydroxy group is further converted into carbonyl through the dehydrogenation reaction catalyzed by a NAD-dependent alcohol dehydrogenase (ADH). Subsequently, a Baeyer–Villiger (BV) oxidation reaction was introduced. Two kinds of esters would form as the results of BV oxidations, and sebacic acid would be obtained as the hydrolysis product of ester compound 5. Among the cascade process, the regioselectivity of the Baeyer–Villiger monoxygenase (BVMO) is the key point. Only part of natural BVMO tend to transfer oxygen atoms to less substituted carbon centers during the catalytic process to generate esters with “abnormal” configurations (compound 5) [8,9]. BVMO from *Pseudomonas aeruginosa* (*Pa*BVMO) [10] and *Pseudomonas fluorescens* DSM 50106 (*Pf*BVMO) [11] were the only two reported enzymes that have “abnormal” regioselectivity fit for sebacic acid production.

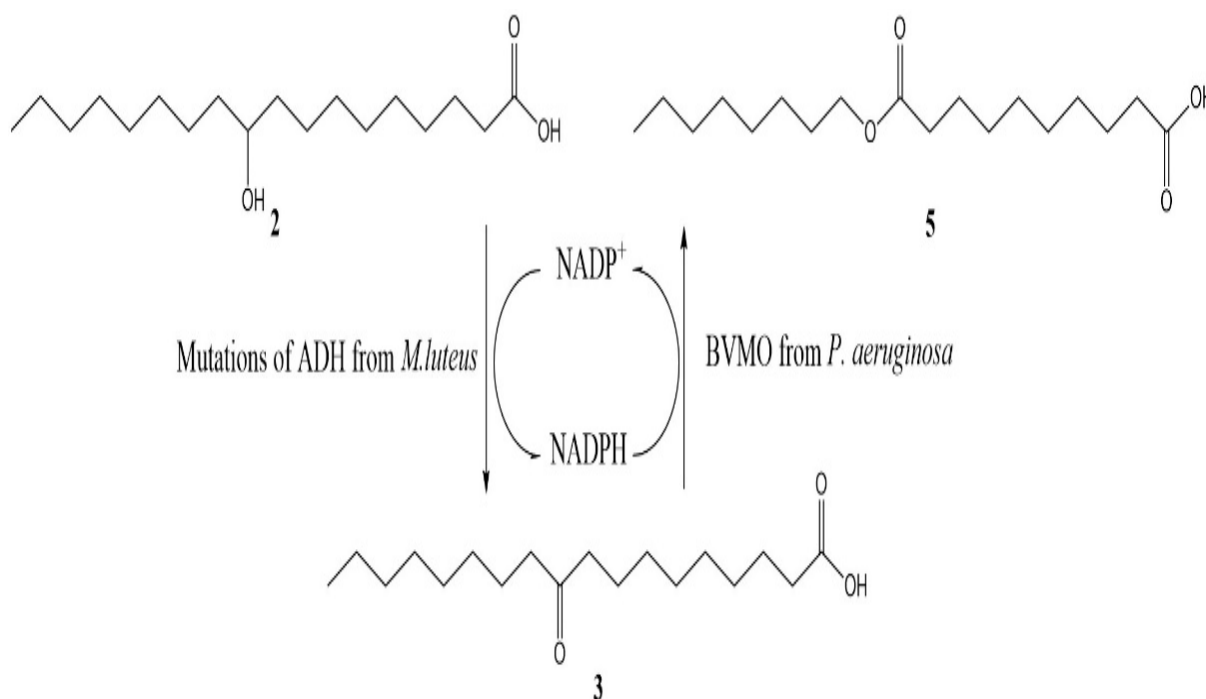


**Scheme 1.** Biotransformation pathway [8]. Oleic acid (1) is converted into either n-nonanoic acid (6) and  $\omega$ -hydroxynonanoic acid (7) or n-octanol (8) and 1,10-decanedioic acid (9) by multistep enzyme-catalyzed reactions.

Beside the regioselectivity of BVMO, there is another limitation for the process. For the biocatalytic cascade of sebacic acid production, the co-factor specificity of two oxidoreductases is different,  $\text{NAD}^+$  was required for ADH, while  $\text{NADP}^+$  was required for BVMO. Thus, it is necessary to introduce other reaction systems for the co-factor regeneration to reduce the cost of this in vitro cascade reactions [12–14]. For example, NADPH regeneration systems, commonly used in BVMO, catalyzed oxidation reactions include glucose-6-dehydrogenase (GDH) [15] and formate dehydrogenase (FDH) [16]. For  $\text{NAD}^+$  regeneration, NADH oxidase (NOX) was the most applied enzymatic regeneration system [17,18]. However, the multiple enzymes operating under uniform reaction conditions may not be optimal for one of the enzymes. The complicated enzymatic cascades require optimization to facilitate the enzyme rate match for maximum catalytic efficiency, and, consequently, the number of enzymes can continue to enhance the multi-enzyme catalysis system. This will not only increase the complexity of the system to match each other but also introduce other by-products, thus, increasing the difficulty of sebacic acid purification. Therefore, construction of a co-factor regeneration system for the cascade reaction of Scheme 1 without additional enzymes is necessary.

The modification of co-factor specificity through protein engineering provides a desired solution for the above problems. Based on the technique of molecular simulation, the mechanism of co-factor switching was investigated [19]. It could be noticed that the structural difference in the phosphate group of the adenosine ribose ring moiety determined the co-factor specificity of oxidoreductases [20,21]. The key residues that influenced the co-factor preference are mainly surrounding around these phosphate group binding sites [22,23]. Rational or semi-rational design works based on the alteration of the size or electrostatic state of the key residues with the help of molecular simulation were carried out for the co-factor switching of virous oxidoreductases. Seo et al. switched the co-factor specificity of secondary alcohol dehydrogenase (*Micrococcus luteus*, *MIADH*) from  $\text{NAD}^+$  to  $\text{NADP}^+$  through a reconstruction of the structure of  $\text{NADP}^+$  binding sites. Then, the engineered enzyme was successfully coupled to a NADPH-dependent BVMO from *Pseudomonas putida* KT2440 for redox-neutral biotransformation of long chain unsaturated fatty acid into medium chain length chemicals [24]. Bommareddy et al. successfully altered the co-factor specificity of glyceraldehyde 3-phosphate dehydrogenase (*Corynebacterium glutamicum*) from  $\text{NAD}^+$  to  $\text{NADP}^+$  dependent [25]. Beier et al. switched the preference of cyclohexanone monooxygenase from *Acinetobacter sp.* NCIMB 9871 from NADPH to NADH by using computational design [26]. Other successful examples included imine reductase [27], secondary alcohol dehydrogenase [28], and dihydrodipicolinate reductase [29], among others.

In this work, an in situ  $\text{NADP}^+$  regeneration system (Scheme 2) is proposed between ADH from *Micrococcus luteus* WIUJH20 (*MIADH*) and *Pa*BVMO by reconstruction of the co-factor binding region of the native *MIADH* from  $\text{NAD}^+$  to  $\text{NADP}^+$  dependent. Thus, a NADPH regeneration system would be built to improve the catalytic efficiency of the multi-enzyme system and to reduce the production costs. The molecular simulation works were carried out for the mutation design. The co-factor preference and its catalytic performance of mutagenesis were also tested. The results of the work are promising to reduce the cost of enzymatic transformations of sebacic acid and the simplified products isolation.



**Scheme 2.** Construction of a NADPH regeneration system by altering the co-factor specificity of a native  $\text{NAD}^+$ -dependent ADH to  $\text{NADP}^+$ .

## 2. Results and Discussion

### 2.1. Probing the Targeted Residues that Determining the Co-Factor Specificity of *MIADH*

The discrimination between  $\text{NAD}^+$ - and  $\text{NADP}^+$ -dependent enzymes is the consequence of differences in the size and structure of the co-factor binding pocket, as well as the physicochemical properties of the surrounding amino acid residues [30]. Initially, a homology model of *MIADH* was built based on the template of a diketoreductase crystal structure (Protein Data Bank code: 4E12, and the sequence identity with *MIADH* is 49.12%) through the SWISS-MODEL (<https://swissmodel.expasy.org>, accessed on 23 May 2019). Then, two steps of molecular docking were performed, with the homology model of *MIADH* as the receptor and  $\text{NAD}^+$  and 10-hydroxyoctadecanoic acid as the ligand, respectively.

From the structure and catalytic mechanism analysis of diketoreductase (PDB code:4E12), three residues of His-Ser-Glu and the active hydrogen from  $\text{NAD}^+$  formed the catalytic triad of the enzyme [9]. From the comparison of docking results (Figures 1 and S2) with the structure of PDB 4E12, the possible active center of *MIADH* should be Ser 126, His 147, and Glu 159. The 10-hydroxyoctadecanoic acid fits into the active site cleft and its 10-hydroxyl group lies between the imidazole ring of His147 and the nicotinamide of  $\text{NAD}^+$ . Another side of the  $\text{NAD}^+$  molecule binds to the enzyme through hydrogen bonds and hydrophobic forces, with the 2' active hydrogen of the nicotinamide moiety of  $\text{NAD}^+$  facing the cleft between the two binding domains, which formed a proton transfer channel between the solution and the active site. The essential difference between  $\text{NADP}^+$  and  $\text{NAD}^+$  is that the 2'-hydroxyl group of the adenosine ribose ring of  $\text{NAD}^+$  is replaced by a phosphate group. It could be noticed that the carboxylate group of Asp 37 forms a hydrogen bond with the 2'-hydroxyl of the adenosine ring of  $\text{NAD}^+$ , which would stabilize the binding of  $\text{NAD}^+$  with the enzyme. However, when the co-factor switched to  $\text{NADP}^+$ , the phosphate group on the adenosine ring may have electrostatic repulsion and steric hindrance with the Asp 37 residue [31]. Therefore, the substitution of Asp 37 by other positively charged and polarized residues may enable  $\text{NADP}^+$  to form hydrogen bonds and stabilize the co-factor binding with the enzyme [32]. In addition, it could be noticed that three other residues Tyr36, Ala38, and Val39 also influenced the interaction between  $\text{NADP}^+$  and peptide chain of *MIADH*, which determined the stability of  $\text{NADP}^+$  in the co-factor binding pocket. Thus,

except for Asp 37, these three residues were also considered as potential targets for further mutation selection.

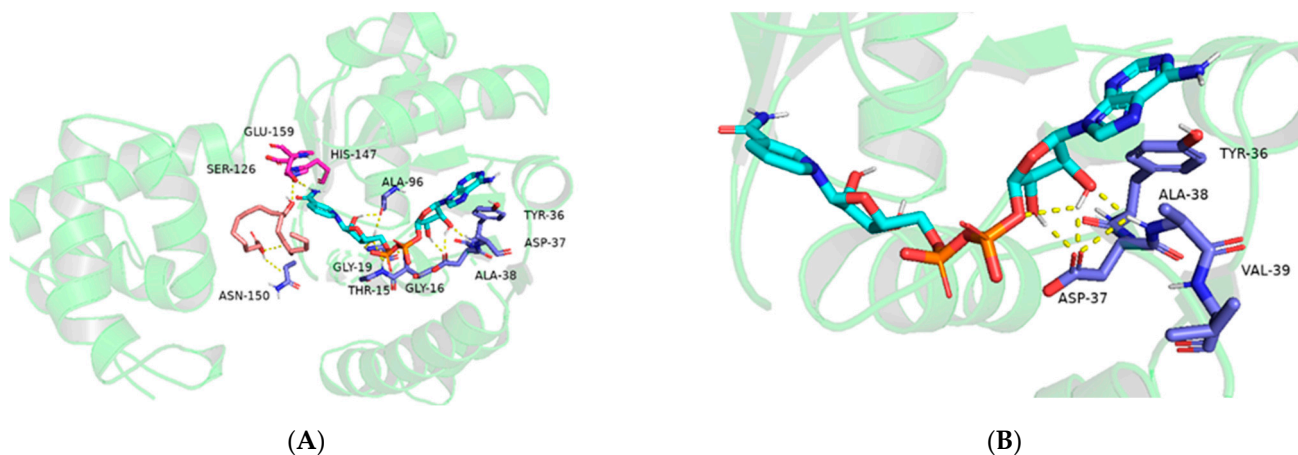


**Figure 1.** Homology modeling and docking analysis of the wildtype *MlADH* complexed with NAD<sup>+</sup>. (A) Enzyme conformation when binding NAD<sup>+</sup> to substrate. (B) Binding force analysis of NAD<sup>+</sup> and enzyme.

Since the site of Asp 37 should be replaced by a small and uncharged residue, glycine and alanine were promising candidates. For the sites of Tyr 36, Ala 38, and Val 39, the residues of serine, threonine, glutamic acid, aspartic acid, lysine, and asparagine were assessed in the investigation. The NADP<sup>+</sup> docking effects of all the possible mutation combinations were simulated. In terms of the docking results of co-factor position, the electron transfer efficiency of co-factor with active site Ser 126 (the distance of active hydrogen of NADP<sup>+</sup> to the hydroxy of Ser 126 is less than 4.5 Å), and the lowest binding energy of the co-factor with enzymes, 6 of the more reasonable candidates (M1: D37G, M2: D37G-V39S, M3: D37G-A38T-V39K, M4: Y36S-D37G-A38D, M5: Y36S-D37G-A38G-V39K, and M6: Y36S-D37G-A38D-V39K) were chosen from 432 possibilities (Figure 2) and were examined in the further experimental characterization.

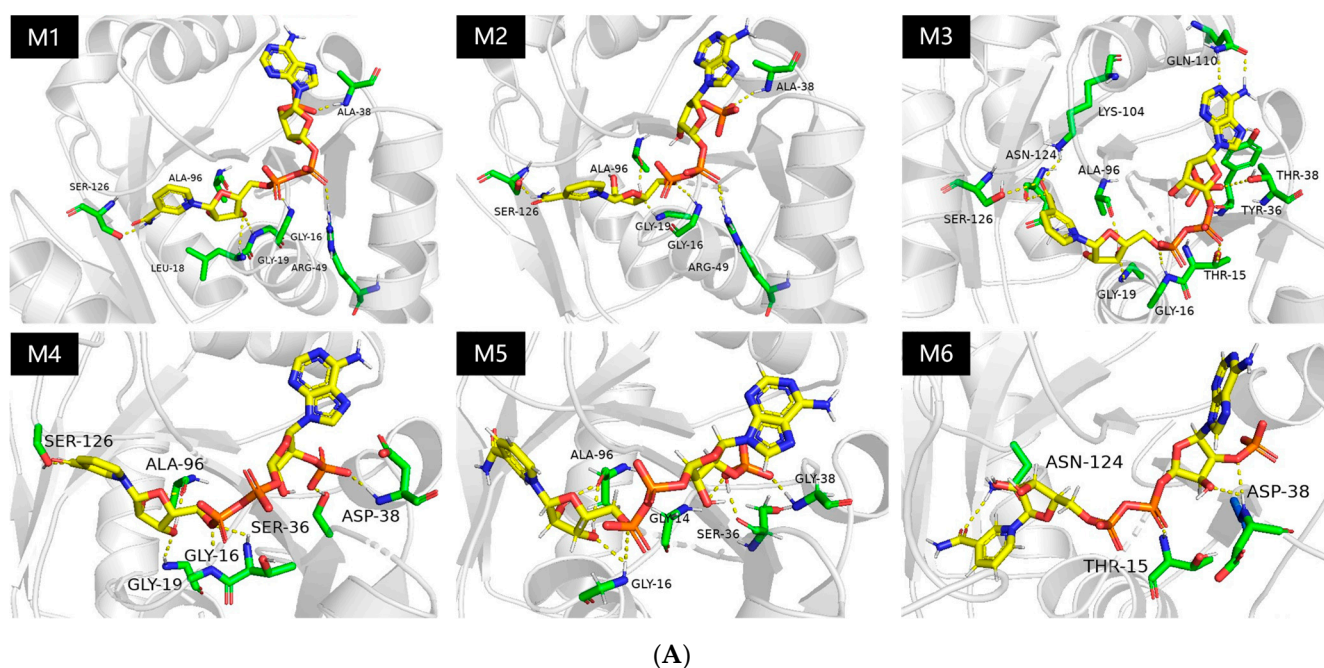


**Figure 2.** Cont.

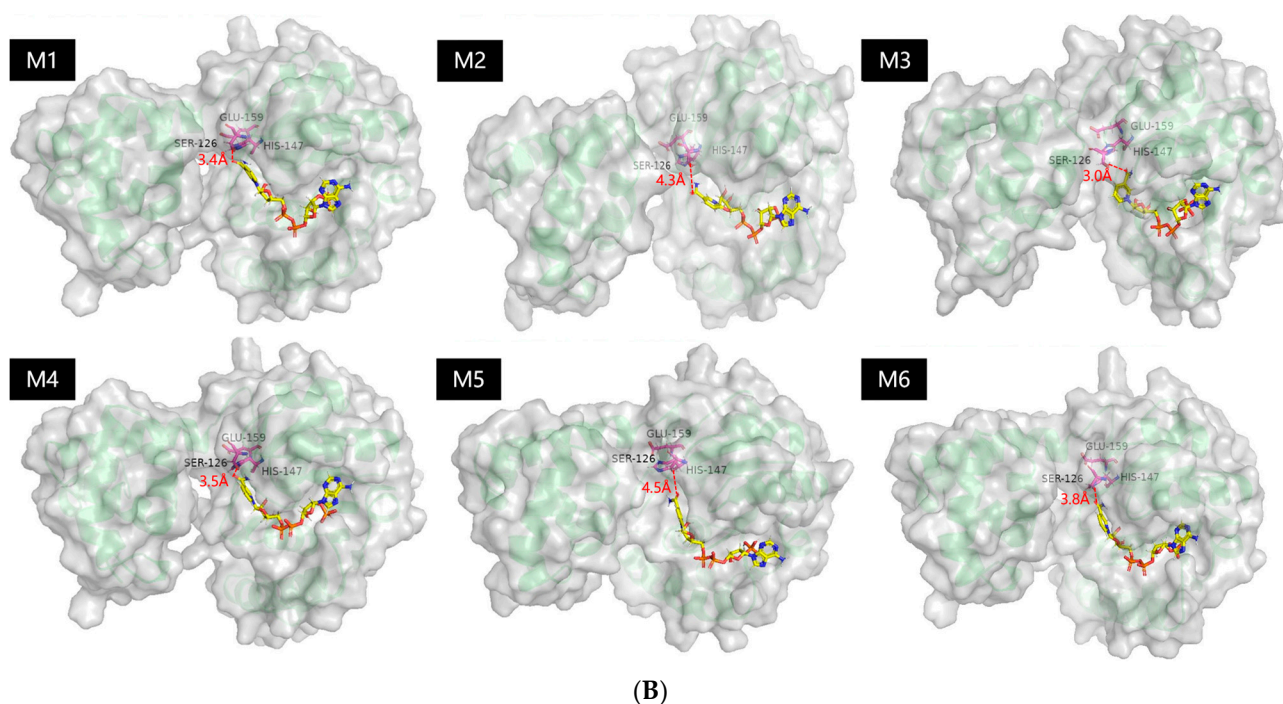


**Figure 2.** Simulation results of reasonable mutation candidates. (A) The binding conformation of NADP<sup>+</sup> in the enzyme; (B) The whole conformation of the ADH with NADP<sup>+</sup>. Mutants of M1 to M6 were D37G, D37G-V39S, D37G-A38T-V39K, Y36S-D37G-A38D, Y36S-D37G-A38G-V39K, and Y36S-D37G-A38D-V39K, respectively.

## 2.2. Enzyme kinetics

Based on the simulation results, six mutational targets were performed through the method of site-directed mutagenesis, and all the engineered protein was heterologously expressed in *E. coli* BL21(DE3). The results of SDS-PAGE indicated that most of the *MIADH* mutants could be successfully expressed; only mutant M4 (Y36S-D37G-A38D) and M6 (Y36S-D37G-A38D-V39K) had relatively low expression rate (Figure 3A,B).

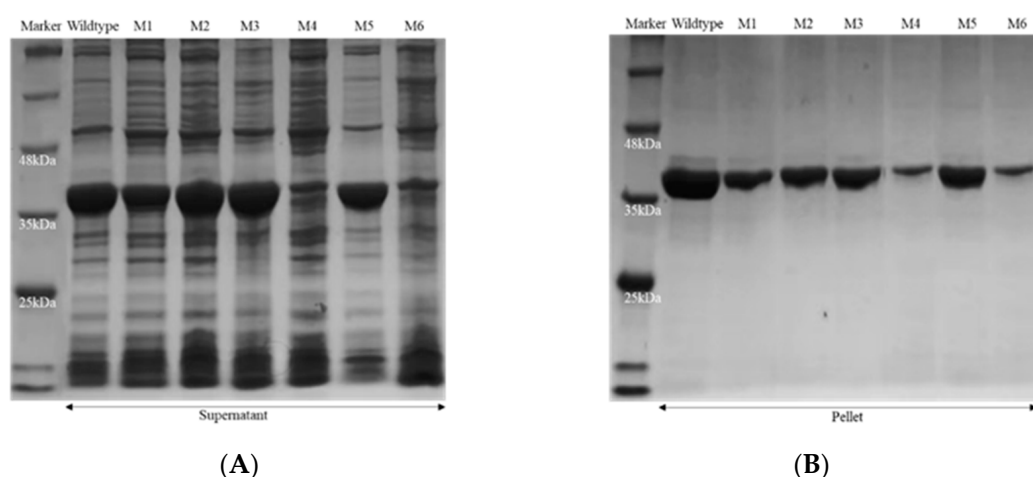


**Figure 3.** SDS-PAGE of the *MIADH* (35.8 kD with a 6×His tag) and its mutant expression in *E. coli* BL-21(DE3). (A) Supernatant; (B) Pellet. Mutants of M1 to M6 were D37G, D37G-V39S, D37G-A38T-V39K, Y36S-D37G-A38D, Y36S-D37G-A38G-V39K, and Y36S-D37G-A38D-V39K, respectively.

In order to investigate the enzymatic properties of each variant, the proteins were purified through Ni-NTA affinity chromatograph. Then, the kinetics parameters were assayed through the dehydrogenation of 10-hydroxyoctadecanoic acid with co-factor of

NAD(P)<sup>+</sup>. Based on the characters that the reduced form of NAD(P)H absorbs at 340 nm, which the aromatic oxidized form does not [33], the changes of the absorbance at 340 nm (OD<sub>340</sub>) along with reaction times were detected. With the substrate-loading variation, the kinetic parameters of each variant were calculated based on the Michaelis–Menten equation and the Hanes–Wolf method [34] (Figure S3).

As shown in Table 1, the wild type of *MIADH* has a good performance with the co-factor of NAD<sup>+</sup> but without detectable activity toward NADP<sup>+</sup>. The mutants of M5 (Y36S/D37G/A38G/V39K) and M6 (Y36S/D37G/A38D/V39K) were more receptive to NAD<sup>+</sup> and unable to utilize NADP<sup>+</sup>. Four other mutants were enabled to utilize NAD<sup>+</sup>/NADP<sup>+</sup> at the same time with preference of NADP<sup>+</sup>. However, the catalytic efficiency ( $k_{cat}/K_m$ ) and the maximum reaction rate ( $V_{max}$ ) of these mutants were reduced, compared with the wild type. Notably, among these mutants, the single point mutation of M1 (D37G) has the best performance with the co-factor switching to NADP<sup>+</sup>, followed by the combinatorial mutation of M3 (D37G/A38T/V39K) and M2 (D37G/V39S). Since the aim of this work is similar to that of Seo et al. [24], the results were compared with them. For the results of Seo et al., the variant of D37S/A38R/V39S/T15I performed the best NADP<sup>+</sup> utilization performance, which is different from ours, and the difference may come from the mutation design method. Meanwhile, the enzyme activity of this investigation was much lower than that of Seo et al. (even for the wild type of *MIADH*). The variation may derive from the difference of strain culture, enzyme purification, and enzymatic reactions. The results of this work could complement the work of Seo et al.

**Table 1.** Enzyme kinetic parameters of wild-type *MIADH* and its variants.

Enzymes	Co-Factors	IU (U·mg <sup>-1</sup> )	$V_{max}$ (mg·mL <sup>-1</sup> min <sup>-1</sup> )	$K_m$ (mM)	$k_{cat}$ (min <sup>-1</sup> )	$k_{cat}/K_m$ (mM <sup>-1</sup> ·min <sup>-1</sup> )
Wildtype	NAD <sup>+</sup>	13.56	4.13	2.08	8.05	3.86
	NADP <sup>+</sup>	*ND	*ND	*ND	*ND	*ND
M1 (D37G)	NAD <sup>+</sup>	1.21	0.02	0.60	0.04	0.07
	NADP <sup>+</sup>	1.82	0.03	0.21	0.05	0.24
M2 (D37G-V39S)	NAD <sup>+</sup>	0.46	0.14	1.56	0.15	0.10
	NADP <sup>+</sup>	0.49	0.15	1.35	0.16	0.12
M3 (D37G-A38T-V39K)	NAD <sup>+</sup>	2.31	0.29	16.48	0.77	0.05
	NADP <sup>+</sup>	0.56	0.07	1.10	0.19	0.17
M4 (Y36S-D37G-A38D)	NAD <sup>+</sup>	0.19	0.06	0.19	0.06	0.30
	NADP <sup>+</sup>	0.19	0.06	0.64	0.06	0.09
M5 (Y36S-D37G-A38G-V39K)	NAD <sup>+</sup>	0.24	0.01	0.04	0.04	0.99
	NADP <sup>+</sup>	*ND	*ND	*ND	*ND	*ND
M6 (Y36S-D37G-A38D-V39K)	NAD <sup>+</sup>	0.30	0.01	0.01	0.05	4.22
	NADP <sup>+</sup>	*ND	*ND	*ND	*ND	*ND

\*ND: not detected. One unit (U) of enzyme activity was defined as the amount of enzyme required to reduce 1 μmol of NAD(P)<sup>+</sup> in 1 min under the assay reaction conditions.

### 2.3. The Efficiency of In Situ NADP<sup>+</sup> Regeneration System for Sebacic Acid Production

Firstly, the dehydrogenation conversion performance of the wild-type *MIADH* with NAD<sup>+</sup> or NADP<sup>+</sup> as co-factors was verified. The conversion rate of 10-hydroxyoctadecanoic acid (**2**) to 10-oxooctadecanoic acid (**3**) was over 98% when NAD<sup>+</sup> was applied, whereas the yields of 10-oxooctadecanoic acid was only 15% when the co-factor changed to NADP<sup>+</sup>. The results indicated that the NADP<sup>+</sup> is not a suitable co-factor for the wild-type *MIADH*. Subsequently, the reactions with three kinds of *MIADH* mutants as catalysts were carried out under the same conditions. When the NADP<sup>+</sup> was utilized as the only source of co-factors, the yields of 10-oxooctadecanoic acid with the mutants M3, M1, M2 as catalysts was 56%, 36%, and 27%, respectively. The results of the dehydrogenation reaction of

10-hydroxyoctadecanoic acid confirmed the switch of the co-factor preference of *MIADH* mutants M3 and M1.

The aim of this investigation was to set up an in situ co-factor regeneration system, which would benefit the biocatalytic cascade of sebacic acid production (Scheme 2). Accordingly, the feasibility of NADP<sup>+</sup> regeneration system of *MIADH* mutants and *PaBVMO* combination was also examined. The traditional multi-enzymatic co-factor regeneration system was set as a controlled group, in which the NOX and the GDH was used for NAD<sup>+</sup> and NADPH regeneration, respectively. As shown in Table 2, the final yield of sebacic acid was 41.2% for the controlled group. The combined catalysis of wild-type *MIADH* and *PaBVMO* still obtained a sebacic acid yield of 20.1% with a single addition of NADP<sup>+</sup>. This may attribute to the weak NADP utilization ability of *MIADH* or from the trace amounts of intracellular NAD<sup>+</sup> in the lyophilized enzymes. Interestingly, the combination of *MIADH* mutants (M1 and M3) and *PaBVMO* with NADP<sup>+</sup> as a co-factor were improved to various degrees, while the sebacic yield of mutant M3 group (49.3%) was higher than the traditional multi-enzymatic co-factor regeneration system (41.2%). Even from the results of Table 1, the kinetic parameters of our variants are not as good as the related work [24]; the usage of these variants in the cascade enzymatic reactions for sebacic acid production (Table 2) demonstrated the capability of these variants to create a cooperative NADP<sup>+</sup> regeneration system with *BVMO*. Thus, the cascade method, combining a proper *BVMO* with *MIADH* variants preferring NADP<sup>+</sup>, might increase the sebacic acid productivity and reduce the cost of the process.

**Table 2.** Yields of sebacic acid by multistep catalytic reactions through different combinations of *MIADH* or its variants and *PaBVMO*.

Enzymes	Co-Factors	Yields of Sebacic Acid (%)
Wildtype <i>MIADH</i> & <i>PaBVMO</i> & NOX & GDH	NAD <sup>+</sup> & NADP <sup>+</sup>	41.2 ± 2.7
Wildtype <i>MIADH</i> & <i>PaBVMO</i>	NAD <sup>+</sup>	6.7 ± 1.2
	NADP <sup>+</sup>	20.1 ± 3.9
M1(D37G) & <i>PaBVMO</i>	NAD <sup>+</sup>	2.1 ± 1.1
	NADP <sup>+</sup>	42.4 ± 2.2
M2(D37G-V39S) & <i>PaBVMO</i>	NAD <sup>+</sup>	5.3 ± 1.4
	NADP <sup>+</sup>	25.8 ± 3.2
M3(D37G-A38T-V39K) & <i>PaBVMO</i>	NAD <sup>+</sup>	2.4 ± 0.8
	NADP <sup>+</sup>	49.3 ± 3.6

Molecular docking was introduced to analyze the benefit reason of above two positive mutants. As shown in Figure 4, the substitution of the amino acid residue of position 37 from Asp to Gly would expand the size of co-factor binding pocket, remove the potential electrostatic repulsion, decrease the effect of steric hinderance, and increase the binding affinity of NADP<sup>+</sup> successfully. Except for position 37, the residue of Val 39 also affected the ADH to accept NADP<sup>+</sup>. However, the mutation of D37G-V39S does not display an obvious effect for the utilization of NADP<sup>+</sup>. For the combinatorial mutation of D37G/A38T/V39K, the simulation result revealed that the substitution of Ala 38 to Thr provide more intermolecular hydrogen bonds between peptide chain and the phosphate of NADP<sup>+</sup>. Meanwhile, from the binding energy analysis results in Table 3, the binding energy of wild-type *MIADH* to NADP<sup>+</sup> is only −14.31 kJ/mol, which was significantly lower than that of each mutant. For each mutant of *MIADH*, the binding energy of NADP<sup>+</sup> with protein changed significantly and comes to the same level of the wild-type *MIADH* with NAD<sup>+</sup> (−34.60 kJ·mol<sup>−1</sup>). Mutant *MIADH*\_D37G-A38T-V39K demonstrated the best results of −34.96 kJ·mol<sup>−1</sup>, which may explain the reversion of the better NADP<sup>+</sup> utilization of *MIADH* mutant M3 (Table 2). However, the worse catalytic results of mutant M2 could

not be explained by the results of the docking simulation, and the reason needs further analysis.

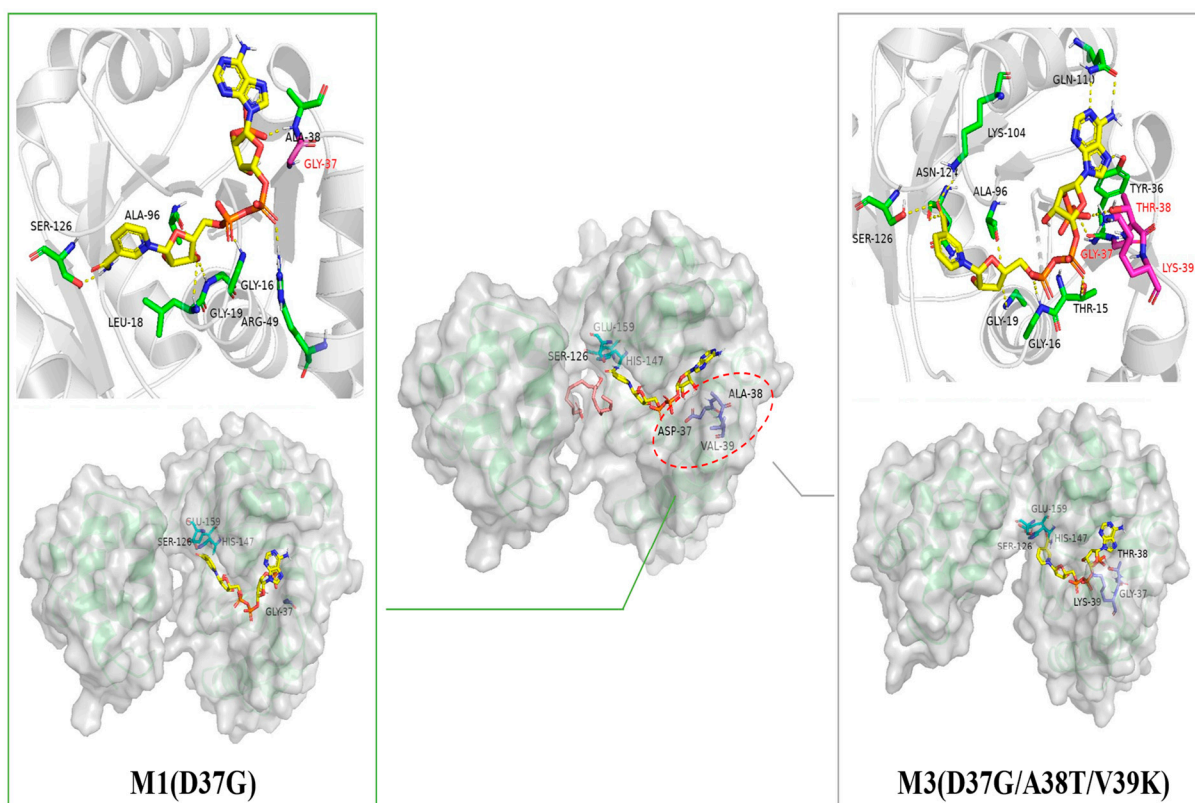


**Figure 4.** Intramolecular interactions and enzyme surface structure analysis of the wildtype *MIADH* complexed with  $\text{NAD}^+$  and its mutants of M1 and M3 complexed with  $\text{NADP}^+$ . The dotted lines represent hydrogen bonds.

**Table 3.** Docking and binding energy of *MIADH* and its mutants to  $\text{NAD(P)}^+$ .

<i>MIADH</i> or Mutants	Co-Factors	Binding Energy ( $\text{kJ}\cdot\text{mol}^{-1}$ )
Wildtype	$\text{NAD}^+$	−34.60
	$\text{NADP}^+$	−14.31
M1(D37G)	$\text{NAD}^+$	−29.79
	$\text{NADP}^+$	−27.69
M2(D37G-V39S)	$\text{NAD}^+$	−30.87
	$\text{NADP}^+$	−32.56
M3(D37G-A38T-V39K)	$\text{NAD}^+$	−31.73
	$\text{NADP}^+$	−34.96

### 3. Materials and Methods

#### 3.1. Materials

The 10-oxooctadecanoic acid and 10-ketostearic acid were purchased from Kaiwei Chemical Technology Co., Ltd. (Shanghai, China). The 10-hydroxyoctadecanoic acid was purchased from Bide Pharmaceutical Technology Co., Ltd. (Shanghai, China). Other chemicals and reagents were purchased from BioRo Yee Ltd. (China), and all of them were of analytical grade. The strain of *E. coli* DH5 $\alpha$  (used for molecular cloning) and *E. coli* BL21 (DE3) (used for gene expression) were purchased from Shanghai Weidi Biotechnology Co., Ltd., China. The site mutation kit of “mut express II fast mutagenesis kit V2” was from Vazyme Biotech Co., Ltd. (China). Plasmid extraction kits and gel extraction kits were obtained from Omega Bio-tek (USA).

### 3.2. Molecular Modeling

Homology models of ADH from *Micrococcus luteus* (NCBI Reference Sequence: ADD83022.1, 310 amino acid residues) were generated based on the structures of dike-toreductase (PDB code: 4E12, 283 amino acid residues) using the molecular modeling platform SWISS-MODEL (<https://swissmodel.expasy.org>, accessed on 23 May 2019) [35], the information of homology model was illustrated in Figure S1. The docking simulations of co-factor-*MIADH* complexes were performed with the YASARA software package (version 21.8.26). With the *MIADH* homology model as the rigid receptor, the cofactor as the flexible ligand, and the carboxyl oxygen of Asp37 as the center, a 25 × 25 docking “box” was set. Then, AMBER 03 force field was used, and docking simulation was carried out at 298K and atmospheric pressure. The docking script “dock\_run.mcr” was run to complete 50 rounds of docking, and the optimal docking conformation was screened according to the binding energy and binding conformation. The conformational clusters with correct docking conformation and the highest binding energy with co-factor were considered for further molecular dynamics (MD) simulations to improve the structure of the model. The MD simulations were carried out in aqueous environments with an AMBER03 force field at a pH of 7.5 and a temperature of 313K for 10 ns.

It should be noticed that there is a new structure of *MIADH* (PDB code: 6KQ9) published. To check the influence of the difference between our homology models from 4E12 and the experiment structure of 6KQ9, a series of simulation works with 6KQ9 as a template were carried out. The results of structure comparison of the homology model from different templates (Figure S7), the comparison of the simulation results of homology model from 4E12 and 6KQ9 (Figure S8), and the details of the structure of NADP<sup>+</sup> binding sites analysis (in Figure S9) indicated that there were not significant alterations between the simulation results in the homology model from 4E12 and the *MIADH* structures of 6KQ9.

### 3.3. Gene Cloning and Expression of Recombinant Enzymes

The gene of *PaBVMO* (BVMO from *Pseudomonas aeruginosa*, NCBI Reference Sequence: WP\_003087250.1) and *MIADH* (ADH from *Micrococcus luteus*, NCBI Reference Sequence: ADD83022.1) was synthesized by Inovogen Ltd. (China), and the sequence was inserted into the plasmid pET28a (+) and pET22b (+) between the NdeI and HindIII restriction nuclease sites, respectively.

Site-directed mutagenesis was performed by the MutExpress II Fast Mutagenesis Kit V2, and the operations were undertaken according to the manufacturer’s instructions. The code of primers utilized for mutagenesis are shown in Table 4.

**Table 4.** Primers used for mutagenesis.

Mutants		Primer
M1(D37G)	F	CGGCACTGCACCATAGGCCATCAC
	R	GGCCTATGGTGCAGTGCCGGC
M2(D37G-V39S)	F	GCTGCCGGGCTTGCACCATAGGCCATCAC
	R	GATGGCCTATGGTGCAAGCCCCGGCAGCAC
M3(D37G-A38T-V39K)	F	GTGCTGCCGGGCTTTGTACCATAGGCCATCAC
	R	GATGGCCTATGGTACAAAGCCGGCAGCAC
M4(Y36S-D37G-A38D)	F	CTGCCGGCACGTCACCACTGGCCATCACTTTTTTG
	R	GTGATGGCCAGTGGTGACGTGCCGGCAGCAC
M5(Y36S-D37G-A38G-V39K)	F	GTGCTGCCGGGCTTCCACCACTGGCCATCACTTTTTTG
	R	GTGATGGCCAGTGGTGGAAGCCCCGGCAGCACTGG
M6(Y36S-D37G-A38D-V39K)	F	GTGCTGCCGGGCTGTCACCACTGGCCATCACTTTTTTG
	R	GTGATGGCCAGTGGTGACAGCCCCGGCAGCACTGG

For expression, the plasmid was transformed into *E. coli* BL21 (DE3). The transformants were cultured in 100 mL TB medium at 37 °C and 200 rpm until the optical

density at 600 nm ( $OD_{600}$ ) reached 0.6–0.8, followed by adding 200  $\mu$ M of isopropyl- $\beta$ -D-thiogalactopyranoside (IPTG), and then cultured at 16 °C for 24 h. After culture, cells were harvested by centrifugation (8000 g, 10 min) and washed twice using Tris-HCl buffer (50 mM, pH 7.5). The crude extract was prepared using sonication (400 W, 15 min), and the soluble expression of recombinant enzymes was analyzed via SDS-PAGE and purified by His-tag through Ni-NTA affinity chromatograph [10].

### 3.4. Enzyme Kinetics Assay

The kinetic measurements were performed by monitoring the absorbance of NAD(P)H at 340 nm on a UV-spectrophotometer (Enspize, PerkinElmer) at 25 °C. The assay mixture (200  $\mu$ L) contained a final concentration of 0.5–2.5 mM of 10-hydroxy-octadecanoic acid, 0.1 mM NAD(P)<sup>+</sup>, 50 mM Tris-HCl buffer (pH 7.5), and an appropriate amount of purified enzyme. The kinetic parameters of the purified enzymes were assayed by the Michaelis–Menten equation and Hanes–Wolf method (Figure S3A–C) [34].

### 3.5. Sebacic acid Production with In Situ NADP<sup>+</sup> Regeneration System

Unless otherwise stated, the enzymatic cascade reaction contains 1.0 mM 10-hydroxyoctadecanoic acid, 1 mM NAD(P)<sup>+</sup>, 10  $\mu$ L Tween 20, 0.5 mg/mL *MIADH* (or its mutants), 1 mg/mL *PaBVMO*. The total volume of reaction was 20 mL (50 mM Tris-HCl buffer, pH 7.5). The reactions were carried out at 25 °C for 24 h.

After reaction, the extraction was carried out with ethyl acetate as solvent. Then, the products were hydrolyzed by KOH (1.0 M) at 80 °C for 2 h [10]. After that, the mixture was acidified to pH 2.0 with diluted HCl, following extraction with 1:1 (*v/v*) ethyl acetate. Finally, the solvent was dried under nitrogen and derived by *N*-methyl-*N*-(trimethylsilyl) trifluoroacetamide (TMS).

Then, the content of sebacic acid as the hydrolytic product of each cascade reaction was measured by GC-MS with following chromatographic conditions. GC-MS (Agilent 7890A-5975C) was equipped with a HP-5 ms capillary column (30 m  $\times$  0.25 mm  $\times$  0.1  $\mu$ m, J&W Scientific Columns, Agilent Technologies, Shanghai, China) [10]. Peaks were identified with a library search of NIST98 and standard sample analysis of each compound. GC-MS results (Figures S4–S6) were quantified using the peak area normalization method, and all measurements were conducted in triplicate.

## 4. Conclusions

Sebacic acid is an important chemical intermediate. With the development of enzymatic technologies, the multi-enzymatic cascade reaction makes it possible to produce sebacic acid from natural oleic acid. However, the problem of co-factor regeneration limited the progress of this biochemical technique. An efficiency and stable co-factor regeneration system for this in vitro enzymatic process is necessary.

In this study, with the switch of co-factor preference of native *MIADH* from NAD<sup>+</sup> to NADP<sup>+</sup> dependent, a NADP<sup>+</sup>/NADPH in situ regeneration system is established between *MIADH* and *PaBVMO*. In silico simulation results indicated that the position of amino acid residue 37 is a key site for the co-factor preference. Except for residue 37, the residue sites of 38 and 39 also influenced the co-factor dependence. The experimental results demonstrated that the mutant of M1(D37G) and M3(D37G/A38T/V39K) would efficiently utilize NADP<sup>+</sup>, and the in situ co-factor regeneration system of *MIADH*\_D37G/A38T/V39K and *PaBVMO* combination has a higher sebacic acid yield than the multi-enzyme regeneration system. All the results indicated that the investigation is beneficial for the sebacic acid production and is helpful for simplifying product isolation, thus, reducing the cost of the enzymatic transformations process. Furthermore, the method could also facilitate the co-factor regeneration system design for other related biotransformation processes.

**Supplementary Materials:** The following are available online at <https://www.mdpi.com/article/10.3390/catal12111318/s1>, Figure S1: Homology modeling results based on 4E12. Figure S2: The structure comparison of *Ml*ADH-NAD<sup>+</sup> with 4E12-NAD<sup>+</sup>. Figure S3: Determination of kinetic parameters by Hanes-Woolf method. Figures S4–S6: GC chromatography of different enzymatic reactions. Figure S7: Structure comparison of homology model from PDB: 4E12 and PDB: 6KQ9. Figure S8: Comparison of simulation results of homology model from 4E12 and 6KQ9 with reasonable mutation candidates. Figure S9: Simulation results of reasonable mutation candidates with PDB 6KQ9 as templet.

**Author Contributions:** J.L. (Jie Luand) and Q.W., performed the experiments. D.L. and S.J., contributed to molecular dynamic simulation. J.L. (Junfeng Liu) and M.Q., analyzed the results. L.D. and F.W., conceived and designed the experiments. K.N., supervised data and wrote the paper together with all authors. All authors have read and agreed to the published version of the manuscript.

**Funding:** This research was funded by National Natural Science Foundation of China (21978017, 21978020, 22078013). The authors would like to offer their thanks for the above funding.

**Conflicts of Interest:** The authors declare no conflict of interest.

## References

1. Zhang, F.; Huang, C.; Xu, T. Production of sebacic acid using two-phase bipolar membrane electro dialysis. *Ind. Eng. Chem. Res.* **2009**, *48*, 7482–7488. [[CrossRef](#)]
2. Köckritz, A.; Martin, A. Synthesis of azelaic acid from vegetable oil-based feedstocks. *Eur. J. Lipid Sci. Technol.* **2011**, *113*, 83–91. [[CrossRef](#)]
3. Kroha, K. Industrial biotechnology provides opportunities for commercial production of new long-chain dibasic acids. *Inform* **2004**, *15*, 568–571.
4. Song, J.W.; Lee, J.H.; Bornscheuer, U.T.; Park, J.B. Microbial synthesis of medium-chain  $\alpha$ ,  $\omega$ -dicarboxylic acids and  $\omega$ -aminocarboxylic acids from renewable long-chain fatty acids. *Adv. Synth. Catal.* **2014**, *356*, 1782–1788. [[CrossRef](#)]
5. Lim, S.; Yoo, H.W.; Sarak, S.; Kim, B.G.; Yun, H. A multi-enzyme cascade reaction for the production of  $\alpha$ ,  $\omega$ -dicarboxylic acids from free fatty acids. *J. Ind. Eng. Chem.* **2021**, *98*, 358–365. [[CrossRef](#)]
6. Garcia-Junceda, E. *Multi-Step Enzyme Catalysis: Biotransformations and Chemoenzymatic Synthesis*; Wiley-VCH: Weinheim, Germany, 2008; pp. 83–107.
7. Mutlu, H.; Meier, M.A.R. Castor oil as a renewable resource for the chemical industry. *Eur. J. Lipid Sci. Technol.* **2010**, *112*, 10–30. [[CrossRef](#)]
8. Song, J.W.; Jeon, E.Y.; Song, D.H.; Jang, H.Y.; Bornscheuer, U.T.; Oh, D.K.; Park, J.B. Multistep enzymatic synthesis of long-chain  $\alpha$ ,  $\omega$ -dicarboxylic and  $\omega$ -hydroxycarboxylic acids from renewable fatty acids and plant oils. *Angew. Chem. Int. Ed.* **2013**, *52*, 2534–2537. [[CrossRef](#)] [[PubMed](#)]
9. Lu, M.; Huang, Y.; White, M.A.; Wu, X.; Liu, N.; Cheng, X.; Chen, Y. Dual catalysis mode for the dicarbonyl reduction catalyzed by diketoreductase. *Chem. Commun.* **2012**, *48*, 11352–11354. [[CrossRef](#)] [[PubMed](#)]
10. Yu, J.-M.; Liu, Y.-Y.; Zheng, Y.-C.; Li, H.; Zhang, X.-Y.; Zheng, G.-W.; Li, C.-X.; Bai, Y.-P.; Xu, J.-H. Direct access to medium-chain  $\alpha$ ,  $\omega$ -dicarboxylic acids by using a Baeyer–Villiger monooxygenase of abnormal regioselectivity. *ChemBioChem* **2018**, *19*, 2049–2054. [[CrossRef](#)] [[PubMed](#)]
11. Kirschner, A.; Altenbuchner, J.; Bornscheuer, U.T. Cloning, expression, and characterization of a Baeyer–Villiger monooxygenase from *Pseudomonas fluorescens* DSM 50106 in *E. coli*. *Appl. Microbiol. Biotechnol.* **2007**, *73*, 1065–1072. [[CrossRef](#)]
12. Wichmann, R.; Vasic-Racki, D. Co-factor regeneration at the lab scale. *Technol. Transf. Biotechnol.* **2005**, *92*, 225–260.
13. Liu, W.; Wang, P. Co-factor regeneration for sustainable enzymatic biosynthesis. *Biotechnol. Adv.* **2007**, *25*, 369–384. [[CrossRef](#)]
14. Zhou, H.; Meng, L.; Yin, X.; Liu, Y.; Xu, G.; Wu, J.; Wu, M.; Yang, L. Artificial biocatalytic cascade with three enzymes in one pot for asymmetric synthesis of chiral unnatural amino acids. *Eur. J. Org. Chem.* **2019**, *2019*, 6470–6477. [[CrossRef](#)]
15. Xu, Z.; Jing, K.; Liu, Y.; Cen, P. High-level expression of recombinant glucose dehydrogenase and its application in NADPH regeneration. *J. Ind. Microbiol. Biotechnol.* **2007**, *34*, 83–90. [[CrossRef](#)] [[PubMed](#)]
16. Bommaris, A.S.; Schwarm, M.; Stingl, K.; Kottenhahn, M.; Huthmacher, K.; Drauz, K. Synthesis and use of enantiomerically pure tert-leucine. *Tetrahedron: Asymmetry* **1995**, *6*, 2851–2888. [[CrossRef](#)]
17. Zhuang, M.-Y.; Jiang, X.-P.; Ling, X.-M.; Xu, M.-Q.; Zhu, Y.-H.; Zhang, Y.-W. Immobilization of glycerol dehydrogenase and NADH oxidase for enzymatic synthesis of 1, 3-dihydroxyacetone with in situ co-factor regeneration. *J. Chem. Technol. Biotechnol.* **2018**, *93*, 2351–2358. [[CrossRef](#)]
18. Xu, M.Q.; Li, F.L.; Yu, W.Q.; Li, R.F.; Zhang, Y.W. Combined cross-linked enzyme aggregates of glycerol dehydrogenase and NADH oxidase for high efficiency in situ NAD<sup>+</sup> regeneration. *Int. J. Biol. Macromol.* **2020**, *144*, 1013–1021. [[CrossRef](#)]
19. Chánique, A.M.; Parra, L.P. Protein engineering for nicotinamide coenzyme specificity in oxidoreductases: Attempts and challenges. *Front. Microbiol.* **2018**, *9*, 194. [[CrossRef](#)]

20. Rodríguez, C.; Lavandera, I.; Gotor, V. Recent Advances in Cofactor Regeneration Systems Applied to Biocatalyzed Oxidative Processes. *Curr. Org. Chem.* **2012**, *16*, 2525–2541. [[CrossRef](#)]
21. Brinkmann-Chen, S.; Flock, T.; Cahn, J.K.B.; Snow, C.D.; Brustad, E.M.; McIntosh, J.A.; Meinhold, P.; Zhang, L.; Arnold, F.H. General approach to reversing ketol-acid reductoisomerase cofactor dependence from NADPH to NADH. *Proc. Natl. Acad. Sci. USA* **2013**, *110*, 10946–10951. [[CrossRef](#)]
22. Yang, F.; Liu, N.; Chen, Y.; Wang, S.; Liu, J.; Zhao, L.; Ma, X.; Cai, D.; Chen, S. Rational engineering of cofactor specificity of glutamate dehydrogenase for poly- $\gamma$ -glutamic acid synthesis in *Bacillus licheniformis*. *Enzym. Microb. Technol.* **2022**, *155*, 109979. [[CrossRef](#)]
23. Cahn, J.K.B.; Werlang, C.A.; Baumschlager, A.; Brinkmann-Chen, S.; Mayo, S.L.; Arnold, F.H. A general tool for engineering the NAD/NADP cofactor preference of oxidoreductases. *ACS Synth. Biol.* **2017**, *6*, 326–333. [[CrossRef](#)]
24. Seo, E.-J.; Kim, H.-J.; Kim, M.-J.; Kim, J.-S.; Park, J.-B. Cofactor specificity engineering of a long-chain secondary alcohol dehydrogenase from *Micrococcus luteus* for redox-neutral biotransformation of fatty acids. *Chem. Commun.* **2019**, *55*, 14462–14465. [[CrossRef](#)]
25. Bommareddy, R.R.; Chen, Z.; Rappert, S.; Zeng, A.P. A de novo NADPH generation pathway for improving lysine production of *Corynebacterium glutamicum* by rational design of the coenzyme specificity of glyceraldehyde 3-phosphate dehydrogenase. *Metab. Eng.* **2014**, *25*, 30–37. [[CrossRef](#)]
26. Beier, A.; Bordewick, S.; Genz, M.; Schmidt, S.; Van Den Bergh, T.; Peters, C.; Joosten, H.J.; Bornscheuer, U.T. Switch in co-factor specificity of a baeyer–villiger monooxygenase. *ChemBioChem* **2016**, *17*, 2312–2315. [[CrossRef](#)]
27. Borlinghaus, N.; Nestl, B.M. Switching the co-factor specificity of an imine reductase. *ChemCatChem* **2018**, *10*, 183–187. [[CrossRef](#)]
28. Thompson, M.P.; Turner, N.J. Two-enzyme hydrogen-borrowing amination of alcohols enabled by a co-factor-switched alcohol dehydrogenase. *ChemCatChem* **2017**, *9*, 3833–3836. [[CrossRef](#)]
29. Xu, J.-Z.; Yang, H.-K.; Liu, L.-M.; Wang, Y.-Y.; Zhang, W.-G. Rational modification of *Corynebacterium glutamicum* dihydrodipicolinate reductase to switch the nucleotide-co-factor specificity for increasing l-lysine production. *Biotechnol. Bioeng.* **2018**, *115*, 1764–1777. [[CrossRef](#)]
30. Bellamacina, C.R. The nicotinamide dinucleotide binding motif: A comparison of nucleotide binding proteins. *FASEB J.* **1996**, *10*, 1257–1269.
31. Corbier, C.; Clermont, S.; Billard, P.; Skarzynski, T.; Branlant, C.; Wonacott, A.; Branlant, G. Probing the coenzyme specificity of glyceraldehyde-3-phosphate dehydrogenases by site-directed mutagenesis. *Biochemistry* **1990**, *29*, 7101–7106. [[CrossRef](#)]
32. Ge, Y.; Song, P.; Cao, Z.; Wang, P.; Zhu, G. Alteration of coenzyme specificity of malate dehydrogenase from *Streptomyces coelicolor* A3 (2) by site-directed mutagenesis. *Genet. Mol. Res.* **2014**, *13*, 5758–5766. [[CrossRef](#)]
33. De Ruyck, J.; Famerée, M.; Wouters, J.; Perpète, E.A.; Preat, J.; Jacquemin, D. Towards the understanding of the absorption spectra of NAD (P) H/NAD (P)<sup>+</sup> as a common indicator of dehydrogenase enzymatic activity. *Chem. Phys. Lett.* **2007**, *450*, 119–122. [[CrossRef](#)]
34. Qin, Y.Z.; Xia, J.; Wang, B.W. *Biological Reaction Engineering*, 2nd ed.; Chemical Industry Press: Beijing, China, 2009; pp. 9–14.
35. Schwede, T.; Kopp, J.; Guex, N.; Peitsch, M.C. SWISS-MODEL: An automated protein homology-modeling server. *Nucleic Acids Res.* **2003**, *31*, 3381–3385. [[CrossRef](#)]